CHAPTER 2. Orbital Evolution and Apsidal Motion Studies - persistent Sources

X-ray binary pulsars are very good candidates to study the orbital evolution and apsidal motion in binaries. When the neutron star has a strong magnetic field ($B \sim 10^{12}$ G), flow of the infalling matter within the Alfven surface is guided by the magnetic field line. The infalling matter will follow the magnetic lines and fall onto the magnetic poles with velocity nearly equal to the free fall velocity and form an accretion column over the magnetic poles. A hot spot is formed at both the poles and high energy photons are emitted from these regions. Inverse Compton scattering of these photons by high energy electrons in the accretion column produces hard X-rays. If the optical depth of the accretion column is low, the radiation comes along the magnetic axis forming a pencil beam whereas if the optical depth is high, radiation escapes tangential to the accretion column forming a fan beam. Since the neutron star is rotating about its rotation axis, the radiation beam directed along the magnetic axis non-aligned with the rotation axis will sweep across the sky. Whenever this rotating beam of radiation is aligned with the line of sight, a pulse of X-ray radiation is detected. We can measure the arrival time of these X-ray pulses. This allows us to measure the orbital elements of the neutron star orbit. The methods to measure the orbital elements and the results of using these methods to study how the orbit elements change with time for few X-ray binary pulsars are described in this and the next chapter.

Neutron stars in X-ray binaries become X-ray bright when mass accretion from a high mass companion star begins. There are some suggestions that before the onset of mass accretion which makes these system X-ray bright, the neutron star might be detectable as a radio pulsar. PSR B1259–63 and PSR J0045–7319 are two such systems with a radio pulsar in binary with a

non-degenerate companion (Johnston et al. 1992; Kaspi et al. 1994). Such systems become X-ray bright when the companion evolves into a giant and mass transfer from the companion on to the magnetised neutron star starts. Also the X-ray binaries having low mass companions are supposed to be progenitors of the millisecond radio pulsars (Bhattacharya & Srinivasan, 1995). The possibility of such a link was established with the discovery of millisecond X-ray pulsars. It is therefore necessary to study the evolution of X-ray binaries so that we can test the many different evolutionary theories. Long term observations of X-ray binary pulsars can also yield the rate of apsidal motion in these systems, which is a function of the mass distribution in the companion star. Therefore the rate of apsidal motion is directly related to the apsidal motion constant of the companion star and can be estimated. Estimating apsidal motion constant of a star is a direct test for the stellar structure models. The first step in doing such studies as listed above is then to measure the orbital parameters of the binary orbit at different epochs and see how these are changing with time. We present in this and the next chapter our work on the binary orbit determination of some X-ray binaries. In this chapter we discuss three persistent X-ray pulsars and in the next chapter we will discuss three transient X-ray pulsars.

The history of the orbital period can tell us much about the physics of stellar components and their mutual interactions. The binary orbits of X-ray binaries evolve mainly due to

1. Mass transfer from the companion star to the neutron star
2. Mass loss from binary system due to stellar winds of the companion star, and/or
3. Tidal interaction between the neutron star and the companion star.
4. Gravitational wave radiation may also cause orbital evolution. However, in HMXBs this effect is likely to be much weaker compared to the effect of mass loss, mass exchange and tidal interaction.

In systems such as Cen X-3 and SMC X-1, extraordinary sensitivity to orbital changes and short orbital evolutionary times scales combine to allow orbital period changes to be measured with high precision. Lecar, Wheeler and McKee (1976) estimated the time taken by tidal torques to circularise the binary orbit after the supernova explosion at the birth of the neutron

star leaves the binary orbit eccentric. They estimated a tidal circularisation time of $< 10^5$ years for Cen X-3 and $< 10^7$ years for Her X-1. Later, the timing studies of X-ray binary pulsars have given estimates of rate of orbital decay in various binary systems (Table 2.1).

Table 2.1 Orbit decay rates of some X-ray Binaries

Source	Decay rate $\dot{P}_{orb}/P_{orb}(yr^{-1})$	Reference
Her X-1	$(-1.32 \pm 0.16)10^{-8}$	Deeter et al. 1991
Cen X-3	$(-1.78 \pm 0.08)10^{-6}$	Kelley et al. 1983
SMC X-1	$(-3.36 \pm 0.02)10^{-6}$	Levine et al. 1993
LMC X-4	$(-9.89 \pm 0.05)10^{-7}$	Naik & Paul, 2004

The rapidly decreasing orbital period in all the above mentioned sources has all been understood mainly due to tidal interactions between the neutron star and its companion. Tidal evolution requires asynchronism between the orbital motion and the rotation of the companion star. Levine et al. (1993) argued that this asynchronism is maintained by the nuclear evolution of the companion star. During the hydrogen shell burning phase, the companion star expands rapidly and this increases the stellar moment of inertia. This results in a decrease in the rate of rotation of the companion star such that it will be rotating more slowly than that required to maintain synchronism with orbital motion. The tidal torques then try to synchronise the orbit resulting in the orbital decay. The rate of orbital decay give estimates for very short orbital evolution of 3×10^5, 5.5×10^5 and 1×10^6 yr for SMC X-1, Cen X-3 and LMC X-4 respectively (Levine et al. 2000).

With RXTE observations we can measure the orbits of binaries with much higher accuracy than what was possible before. For some systems with very small eccentricity, for which only upper limits on the eccentricity were known, we can now measure the eccentricity and hence also the longitude of periastron. In the next section the method of analysis for timing studies of such systems is described. Section 3 and 4 give the results of our analysis of Cen X-3 and SMC X-4 respectively. Section 5 describes the analysis and results of the 4U1538-52 system which was previously believed to have a circular orbit (Rubin et al. 1997) and later found to have an eccentric orbit (Clark 2000). Our RXTE observations of this system confirm an

eccentric orbit for this system and we also measure a possible rate of apsidal motion of this system.

2.1 Timing analysis for sources with small eccentricity

The arrival times of pulses from a neutron star in binary orbit are modified due to its motion in the orbit. When the neutron star is moving towards the observer the pulses arrive faster and when it is moving away from the observer pulses are delayed. These variations in the arrival times of pulses can be used to determine the orbit of the neutron star. If t'_n is the emission time of the pulses, it can be represented as

$$t'_n = t_0 + nP_{spin} + \frac{1}{2}n^2\dot{P}_{spin}P_{spin} \tag{2.1}$$

Here P_{spin} and $\dot{P}_{spin}$ are the spin period and the spin period derivative of the neutron star at the time t_0. The arrival time of the pulses are related to the emission time of the pulses as

$$t_n = t'_n + f_{orb}(t'_n) \tag{2.2}$$

f_{orb} is a function depending on the orbital elements of the neutron star orbit. In this section we will be discussing the analysis followed to determine orbital elements of orbits that have a very small value of the eccentricity i.e, nearly circular orbits. For such orbits the appropriate orbital elements are

- $a_x \sin i$: projected semi major axis
- E : Epoch when the mean longitude is equal to 90^0
- ω : longitude of periastron, measured from the ascending node
- e : eccentricity of the orbit
- P_{orb} : Orbital period

For a circular orbit the function f_{orb} is given by

$$f_{orb} = a_x \sin i \cos l_n$$

$$l_n = 2\pi(t'_n - E)/P_{orb} + \pi/2 \tag{2.3}$$

It must be noted here that l_n is the mean orbital longitude at time t'_n and is defined such that for an orbit with finite eccentricity and hence a definite ω, l is related to the mean anomaly, M, by $l = M + \omega$. This definition of l ensures that the mean and true longitudes agree at the apsides and it also remains well defined as the eccentricity vanishes, which is not true for mean anomaly. Once we have measured the arrival times for a particular source we can solve equation 2.3 with the method of least squares and get initial estimates for $a_x \sin i$, E and P_{orb}. The residuals are then computed by subtracting the arrival times calculated using the initial estimates from the observed arrival times. The residue will show variations if the orbit has measurable small non-zero eccentricity and/or if the initial estimates are not very accurate. In such a case the residues can be corrected for by introducing the terms initially dropped from the function f_{orb} namely ω and e and the terms for differential corrections to the initial estimates of $a_x \sin i$, E and P_{orb}. Such a function is given by,

$$\begin{aligned}
\delta t_n &= \delta t_0 + n\delta P_0 + \frac{1}{2}n^2 P_0 \dot{P}_0 \\
&\quad + \delta x \sin l_n - \frac{2\pi x}{P_{orb}}\delta E \cos l_n \\
&\quad + \frac{2\pi x}{P_{orb}^2}\delta P_{orb}(t'_n - E)\cos l_n \\
&\quad + \frac{3}{2}xe\sin\omega + \frac{1}{2}xe\cos\omega\sin 2l_n \\
&\quad - \frac{1}{2}xe\sin\omega\cos 2l_n
\end{aligned} \tag{2.4}$$

See appendix A for the detailed deduction of the above equation. Substituting $g = e\sin\omega$ and $h = e\cos\omega$ makes equation 2.4 fully linear in the differential corrections and small parameters. Thus the full problem contains eight parameters and can be solved by the method of linear least-squares. The procedure outlined above should be iterated until satisfactory convergence is achieved. If initial estimates are appropriate generally a single iteration will suffice. The problem is further simplified by freezing the orbital period P_{orb}. Orbital periods given by combining the past observation history of orbital epochs E_n's are more accurate than the once

derived from a single data set. A more accurate P_{orb} can be determined as follows. Past observations by other observers and with other X-ray observatories and/or with RXTE would have reported the E_n values. For a constant rate of change of the orbital period we will get a quadratic variation in the E_n time delays. The time of the n th orbital epoch E_n is given by,

$$E_n = E_0 + nP_{orb} + \frac{1}{2}n^2 P_{orb}\dot{P}_{orb} \tag{2.5}$$

Solving for the above equation by combining the past and new value of orbital epochs will give a more accurate value for P_{orb} and $\dot{P}_{orb}$. The error estimates for all the orbital parameters determined from the method described above for sources with nearly circular orbit, are derived from the diagonal terms of the final covariance matrix that comes by fitting the data with the appropriate equation by linear least square method.

2.2 Cen X-3

Cen X-3 is a high-mass X-ray binary and its pulsar nature was first discovered with *Uhuru* (Scherier et. al. 1972; Giacconi et al. 1971). It has a spin period of ~ 4.8 s and an orbital period of ~ 2.1 days decaying at the rate of $(-1.78 \pm 0.08)10^{-6}\ yr^{-1}$ (Kelley et al. 1983). The binary system consists of a neutron star with mass $1.21 \pm 0.21 M_{\odot}$ and a companion 06-8 III supergiant star of mass $20.5 \pm 0.7 M_{\odot}$ (Hutchings et al. 1979; Ash et al. 1999). The distance of the binary system has been estimated to be roughly 8 kpc, with a lower limit of 6.2 kpc (Krzeminski 1974). We present in this section the analysis of the RXTE-PCA observation of Cen X-3 spanning two binary orbits. Cen X-3 was observed in 1997 using RXTE-PCA for 3.8 days from February 28 to March 3. Twelve pointed observations were made with five Proportional Counter Units (PCU) for most of the time except two occasions when only 4 PCU were used. Apart from the usual data modes Standard-I mode and Standard-II, data was also recorded in 2 single bit mode, 1 binned mode and 1 event mode data. The two single bit mode data together covered the energy range from 1 to 16 keV with 62 microsec time resolution, the binned mode data also covered the same energy range with time resolution of 16 milliseconds

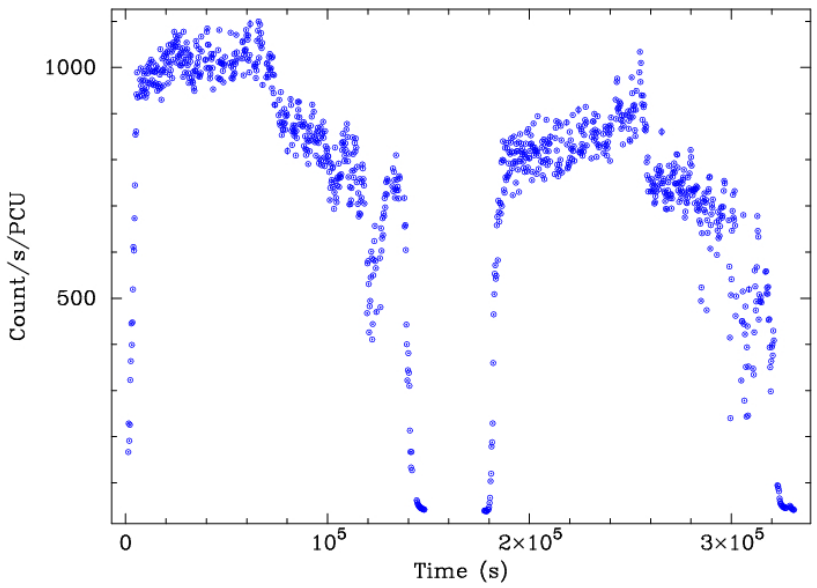

Figure 2.1 Figure shows light curve of Cen X-3 for the 1997 observation made using RXTE-PCA. The light curve was generated using photons from only the first PCU

and the event mode data covers the energy range above 16 keV with a time resolution of 31 microseconds. Figure 2.1 shows the complete light curve of this observation.

2.2.1 Pulse profile variations in Cen X-3

For pulse timing analysis the pulse profile of the neutron star should be stable. If the pulse profile is variable then it will introduce error in measuring the arrival time of the pulses, since it would be difficult to have a unique time marker in the pulse profile. So before we go into further detailed discussion of orbit analysis, we first took a look at the pulse shape and its evolution with time if any. Cen X-3 shows variations in its pulse profile which are not very correlated with the source luminosity whereas the pulse fraction is correlated with the source luminosity. A detailed discussion of this will be given in chapter four of the thesis. Here we are not interested in the global pulse profile changes of Cen X-3. Rather we are interested to see if there are any pulse profile changes in this particular observation which could affect our measurement of pulse arrival times. For this we created a template pulse profile from each pointed observation of which there are twelve between 28th February and 3rd March 1997. Excluding the eclipse,

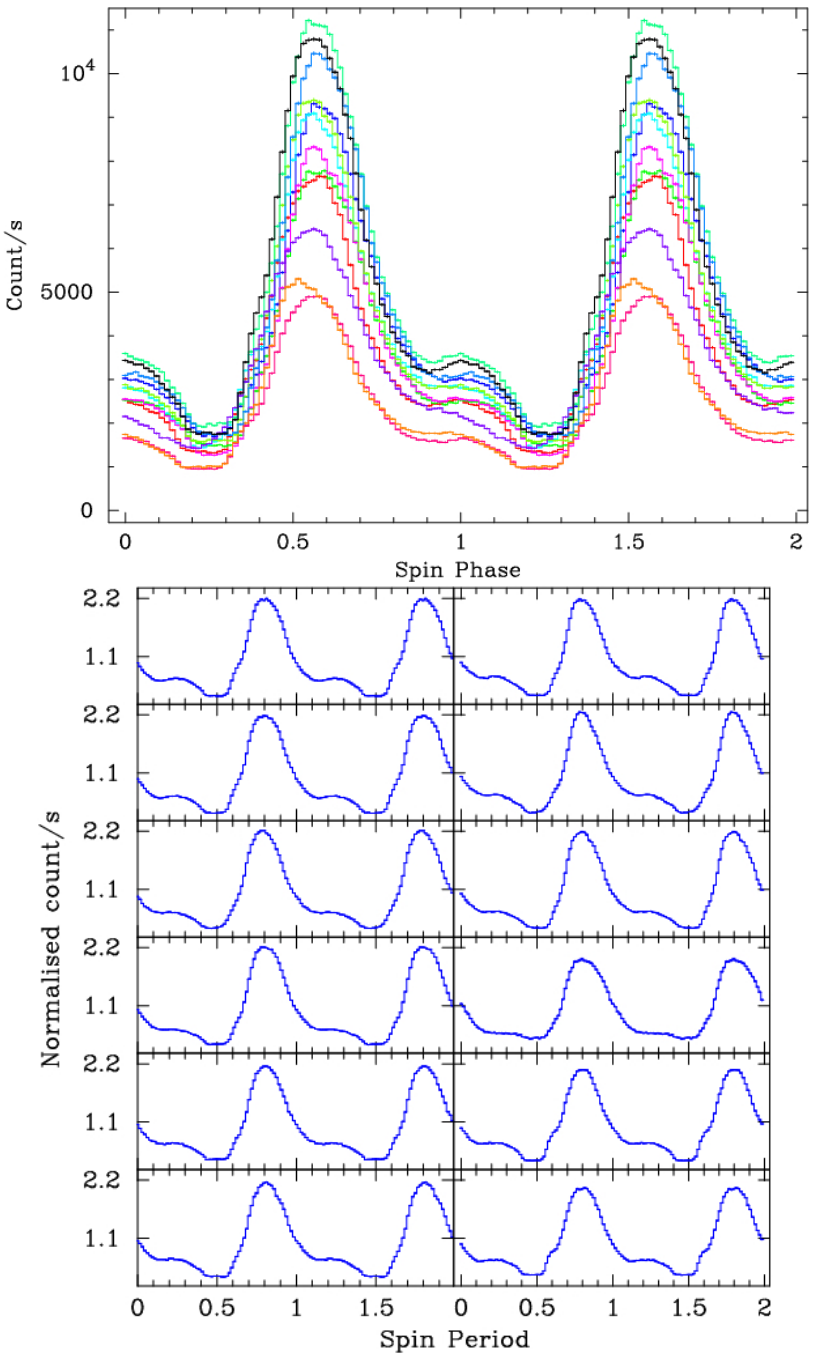

Figure 2.2 Sample pulse profiles of Cen X-3, each from the twelve pointed observations are shown with different colours. The minimum count rate profiles are from times just before and after the central source went into and came out of the eclipse. Ratio of the maximum of primary peak to the maximum of secondary peak remains almost a constant

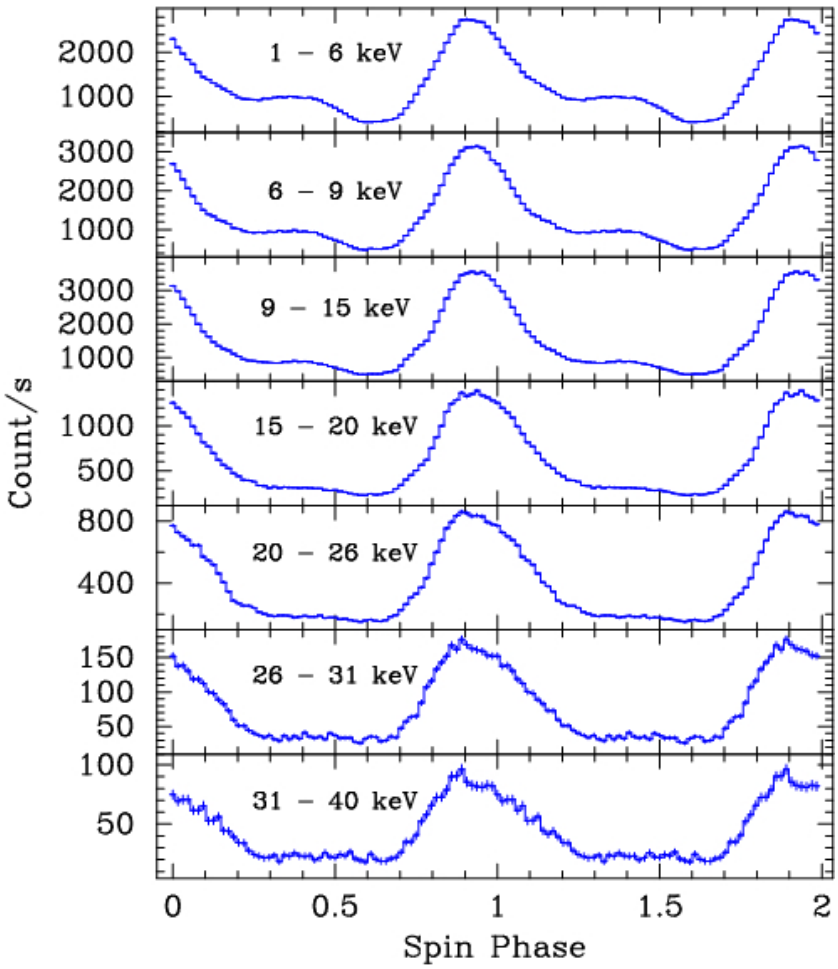

Figure 2.3 Pulse profiles of Cen X3 at different energy ranges folded with the local spin period and averaged over 100 consecutive pulses are shown. The primary peak remains almost similar at all energies but the secondary peak vanishes at higher energies.

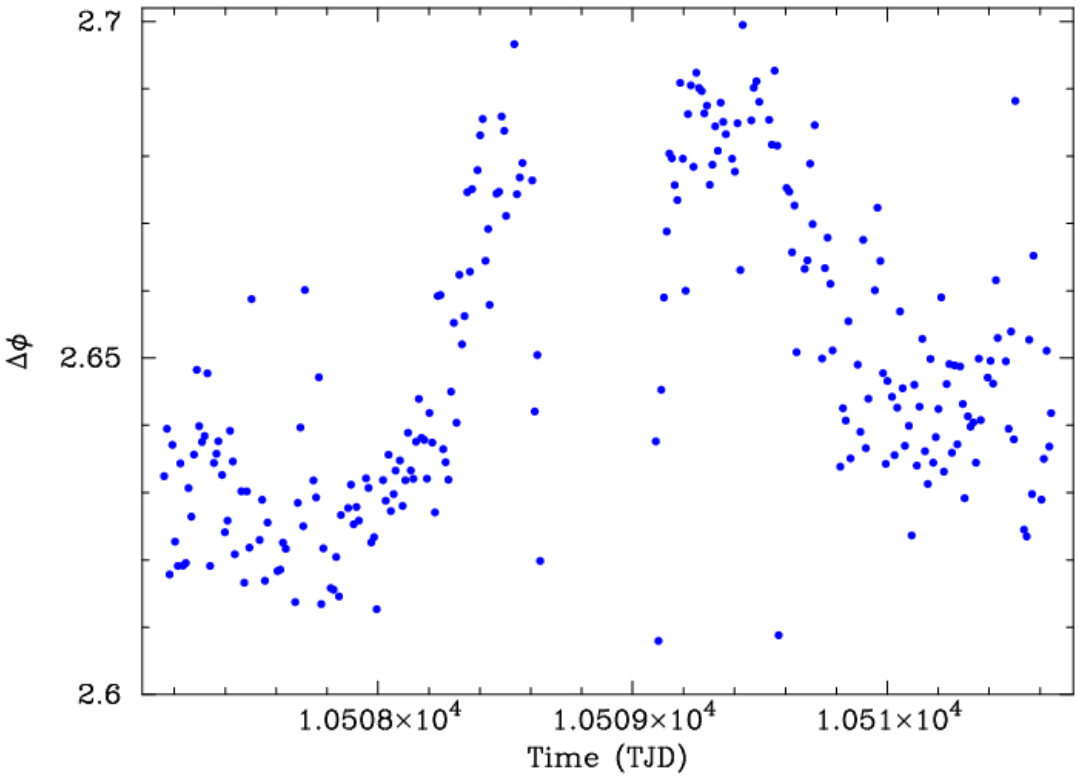

Figure 2.4 Difference in spin phase of primary peak and secondary peak $\Delta\phi$ of Cen X-3 pulse profile is plotted as a function of observation time. The structure seen in the plot shows that $\Delta\phi$ is not a constant indicating that the spin phase of primary peak and secondary peak are not locked and hence can introduce errors in the pulse arrival time analysis.

the instantaneous flux of Cen X-3 varies by a factor of nearly 2 during one orbital cycle. As the neutron star is obscured by the companion star we receive more scattered X-rays during the eclipse, eclipse ingress and eclipse egress , due to which the pulse fraction varies. Figure 2.2a is a plot of the twelve pulse profiles, with the peak positions aligned. To begin with, light curves were generated with time resolution of 15.625 ms and the times were corrected to the solar system barycentre. Each light curve was then searched for the local spin period. Pulse profiles shown in Figure 2.2 are generated by folding the light curve generated from individual pointed observations with the local spin period. Hundred consecutive pulses were averaged together to generate every pulse profile. Overall the pulse profiles look similar, except for the count rates. The pulse profile consists mainly of two peaks, we will call the highest peak as the primary peak and a second smaller peak, which we will call the secondary peak. Figure 2.3b shows the normalised pulse profile for the twelve pointed observations. We also did an energy resolved study of pulse profiles for the observation when the observed source flux was highest (obs-id: 20104-01-01-002). We see that for higher energy ranges, the secondary peak vanishes but the primary peak remains the same (Figure 2.3). Since we intended to use this observation to look for small eccentricity, if any, in the neutron star orbit, we have to know if there are any small variations in pulse profile which cannot be recognised by just looking at the pulse profiles at various times. The difference in the spin phase of the primary peak and the secondary peak which we will call $\Delta\phi$ can give a good measure of small variations in pulse profile. To find $\Delta\phi$ we first Fourier transformed the pulse profiles and noted the phase of the first highest Fourier component ϕ_1 and the second highest Fourier component ϕ_2. The difference between ϕ_1 and ϕ_2 gives $\Delta\phi$. Figure 2.4 shows the variation in $\Delta\phi$ as a function of observation time. The evolution in pulse profile can be explained as arising due to the orbital phase dependant absorption of the soft X-rays. More of the soft X-rays will be absorbed at orbital phases close to the eclipse phase since the X-rays emitted by the neutron star have to pass through a higher absorption column density of the stellar wind of the companion star. This possibility is also supported by the energy resolved pulse profiles. Pulse profile at higher energy do not show the secondary peak, whereas pulse profile at lower energy show the secondary peak (Figure 2.3).

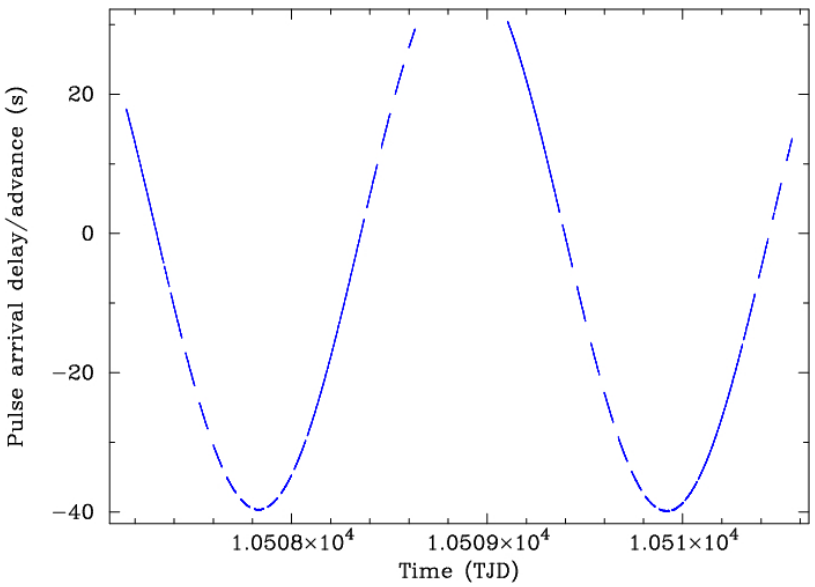

Figure 2.5 The arrival time delay/advance of pulses of Cen X-3 is plotted as a function of time. The two orbits are clearly seen separated by an eclipse when no delay measurements are possible. This curve is used to solve the equation 2.3 and hence measure the orbital elements.

This shows that for the secondary peak the soft X-ray photons contribution is maximum. The accuracy of our pulse arrival time measurement will be limited by these variations in the pulse profile.

2.2.2 Timing analysis

All timing analysis was done using the binned mode data which has a time resolution of 15.625 ms and an energy range of 1-35 keV. Observations carried out during the source eclipse were not used. The photon arrival times in the light curve were corrected to the solar system barycenter. Individual pulse profiles were generated using ten consecutive pulses. The pulses were Fourier transformed and the phase of the frequency component with the highest amplitude was used as the time marker. The arrival time delay of that pulse was then calculated using the product of the phase of highest frequency component and spin period of the neutron star. Figure 2.5 shows the pulse arrival time delay curve for Cen X-3.

This delay curve was then used to solve equation 2.3. The projected semi-major axis and

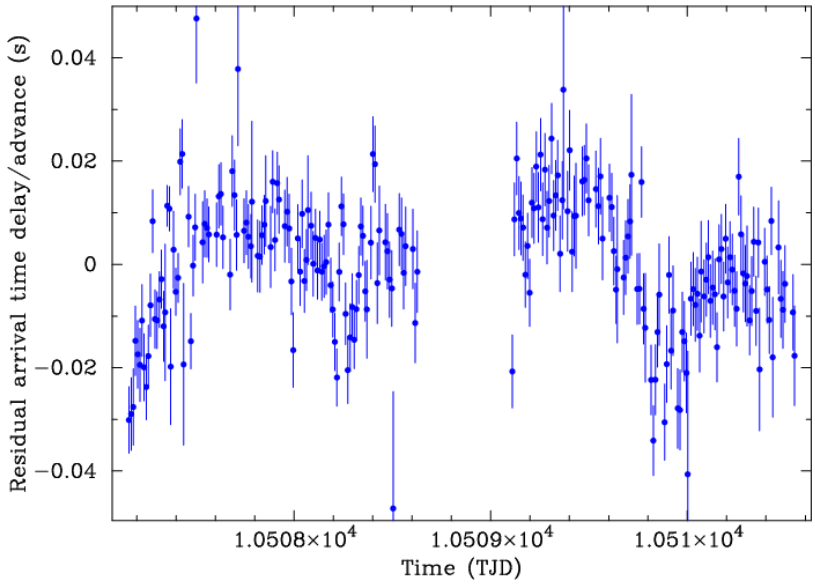

Figure 2.6 The residual arrival time delay/advance of pulses of Cen X-3 are plotted as a function of time. The residues are obtained by subtracting the model arrival times expected due to a circular orbit from the observed pulse arrival delay curve

epoch E were free parameters and the values we get for them are tabulated in Table 2.2. The residual delay and advance in the arrival time of pulse are calculated by subtracting the calculated delays from the observed delays. Figure 2.7 shows the measured residual delays and advances. To clearly bring up the structure in the residual we have averaged fifteen consecutive data points to get one point. The structure in the residue may be due to both a small eccentricity and a variable pulse profile which limits the accuracy with which we can measure the arrival time of the pulses. A residual only due to a small eccentricity of the orbit would have been sinusoidal with a period half the orbital period of the neutron star. The error in the pulse arrival times and the residue due to a finite eccentricity cannot be separated out. Hence we could not measure any eccentricity of Cen X-3 orbit using this data set.

Combining the new value of E with the previous measurements made by other authors (see Table 2.3) we solve equation 2.5 and get more accurate values of the free parameters P_{orb} and $\dot{P}_{orb}/P_{orb}$ (see Table 2.2). Kelley et al. (1983) have analysed the different scenarios that can possibly explain the rate of orbital delay in Cen X-3. They conclude the following :

• $\dot{P}_{orb}/P_{orb}$ only due to conservative mass transfer ($\dot{P}_{orb}/P_{orb} = -1.7 \times 10^{-8} yr^{-1}$) is two orders

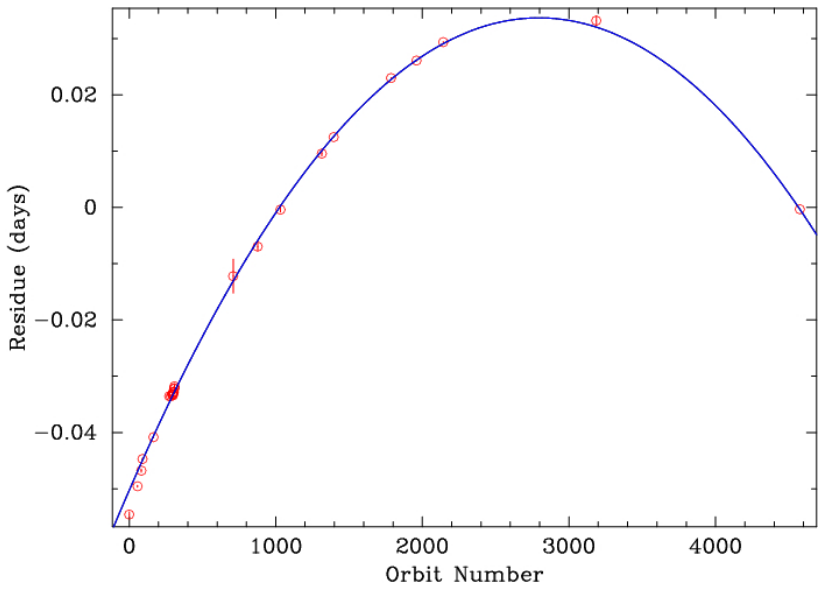

Figure 2.7 The observed-minus-calculated eclipse times are plotted with respect to the orbit number of Cen X-3. The quadratic trend due to orbital period decay is clearly seen. The solid curve represents the best-fit to a constant rate of orbital decay.

Table 2.2 Cen X-3 orbit parameters measured using 1997 RXTE observations

Parameter	Value
$a_x \sin i$	39.6612 ± 0.0009 (lt-sec)
E	$50506.788423 \pm 0.000007$ (MJD)
E_0	958.550276 ± 0.0006 (MJD)
P_{orb}	$2.08713936 \pm 0.00000007d$
$\dot{P}_{orb}/P_{orb}$	$-(1.799 \pm 0.002) \times 10^{-6} yr^{-1}$

Table 2.3 Cen X-3 orbital epoch history

Orbital Cycle	Time JD - 2,440,000.0	Reference
0	958.84643 ± 0.00045	Fabbiano & Schreier 1977
57	1077.81497 ± 0.00015	Fabbiano & Schreier 1977
83	1132.08181 ± 0.00029	Fabbiano & Schreier 1977
91	1148.78051 ± 0.00016	Fabbiano & Schreier 1977
166	1305.31533 ± 0.00014	Fabbiano & Schreier 1977
273	1528.64010 ± 0.00030	Fabbiano & Schreier 1977
284	1551.59798 ± 0.00017	Fabbiano & Schreier 1977
293	1570.38199 ± 0.00011	Fabbiano & Schreier 1977
295	1574.55610 ± 0.00013	Fabbiano & Schreier 1977
296	1576.64330 ± 0.00010	Fabbiano & Schreier 1977
297	1578.73037 ± 0.00007	Fabbiano & Schreier 1977
298	1580.81722 ± 0.00009	Fabbiano & Schreier 1977
300	1584.99193 ± 0.00010	Fabbiano & Schreier 1977
303	1591.25328 ± 0.00015	Fabbiano & Schreier 1977
304	1593.34025 ± 0.00015	Fabbiano & Schreier 1977
307	1599.60212 ± 0.00015	Fabbiano & Schreier 1977
308	1601.68930 ± 0.00014	Fabbiano & Schreier 1977
309	1603.77671 ± 0.00021	Fabbiano & Schreier 1977
709	2438.628 ± 0.003	Tuohy 1976
876	2787.1755 ± 0.0007	van der Klis, Bonnet-Bidaud, & Robba 1980
1032	3112.76642 ± 0.0004	Kelly et al. 1983
1314	3701.33275 ± 0.00043	Howe et al. 1982
1395	3870.38910 ± 0.00002	Kelly et al. 1983
1786	4686.44760 ± 0.00005	Murakami et al. 1983
1960	5049.6025 ± 0.0001	Nagase et al. 1984
2142	5429.45421 ± 0.00005	Nagase et al. 1984
3186	7608.3688 ± 0.0008	Nagase et al. 1992
4575	$10507.288423 \pm 0.000007$	present work

of magnitude smaller than that observed for Cen X-3.

• To explain the observed orbital decay by mass loss from the binary system, the mass loss rate required is $3 \times 10^{-6} M_{\odot} yr^{-1}$. They argue that such high mass outflow in a thin disk or stream like structure would give rise to very high column densities of the order of $10^{26} cm^{-2}$, and would have been detected in orbital phase dependent X-ray and optical studies. Therefore mass loss from the binary system in itself seems to highly unlikely to explain the observed orbital delay.

• Tidal interactions can account for the observed rate of orbit decay. The orbit circularisation time due to tidal interactions are of the order of $1 \times 10^4 yr$. But for tidal interactions, the companion Krezeminski's star must rotate asynchronously with the orbit. This can be achieved by the self-generating tidal instability as first proposed by Darwin (1879). The moment of inertia of the Krezeminski's star about its center of mass is $0.5 \pm^{0.82}_{0.18}$. For a binary system, having components of constant masses and radii, the equilibrium configuration will be unstable if the rotational angular momentum of the companion is larger than one-third the total orbital angular momentum. The orbit of such a system will either expand to reach a second equilibrium or may decay until the two stars coalesce (Darwin 1879). For the Cen X-3 case this scenario is more complicated because the Krezminski's star is losing mass and as it evolves, its radius and internal structure will change. Thus it seems plausible that the evolving Krezminski's star can maintain the asynchronism required for the tidal interactions to explain the observed orbit decay.

Our results for P_{orb} and $\dot{P}_{orb}/P_{orb}$ are consistent with those derived by Kelly et al. (1983). The P_{orb} and $\dot{P}_{orb}/P_{orb}$ have better accuracy than previously reported in literature. Future measurements of orbital ephemeris (E_n) can be used to measure the deviations, if any, from a constant rate of orbital decay. Whether such deviations can be explained by only tidal interactions is not very clear at present.

2.3 SMC X-1

SMC X-1, discovered with *Uhuru* is a high-mass X-ray binary (Leong, et al. 1971) consisting of a neutron star of spin period 0.71 s (Lucke et al. 1976) and a young B0 supergiant companion (Webster et al. 1972, Liller 1973). There are clear X-ray eclipses which occur once every orbital period. The orbital period is 3.892 days (Schreier et al. 1972). This system was observed using RXTE in 2000 and 2003. We present in this section the orbital measurements of this binary for both these years. During the 2000 observation the source was in its high state and hence with this data we could measure the very small eccentricity of the orbit and also for the first time we measured the longitude of periastron of this source. The 2003 observation falls during the low state of the source and could not be used for measuring the eccentricity or the longitude of periastron (Figure 2.8). Figure 2.9 shows the light curve of SMC X-1 for the 2000 and 2003 observation.

2.3.1 Pulse profile variations in SMC X-1

The pulse profile of SMC X-1 is almost sinusoidal, with the second peak amplitude lesser than the main first peak amplitude. Figure 2.11 shows the pulse profile of SMC X-1 for each pointing of the 2000 observation. Each profile is generated by folding the background subtracted light curve with the local spin period. The time resolution of the light curve is 16 ms. The photon arrival times in the light curves were corrected to the solar system barycenter time before folding. To make Figure 2.11 the pulse profiles generated by epoch folding have been multiplied by constants such as to show individual profiles from each pointing clearly. The pulse profile is stable and does not show any sharp variations at different orbital phases. Similar to what we have done for Cen X-3 pulse profile study, we have calculated $\Delta\phi$ for the SMC X-1 pulse profiles also. The two phases used here to calculate $\Delta\phi$ correspond to the main peak and the secondary peak. Figure 2.12 a and b show variations with time in $\Delta\phi$ for the 2000 and 2003 observations of SMC X-1. There are no systematic variations in $\Delta\phi$ for the 2000 observations. But the 2003 observations show a systematic variation in $\Delta\phi$ and hence limit the possibility of measuring the eccentricity and ω of the SMC X-1 orbit using that data.

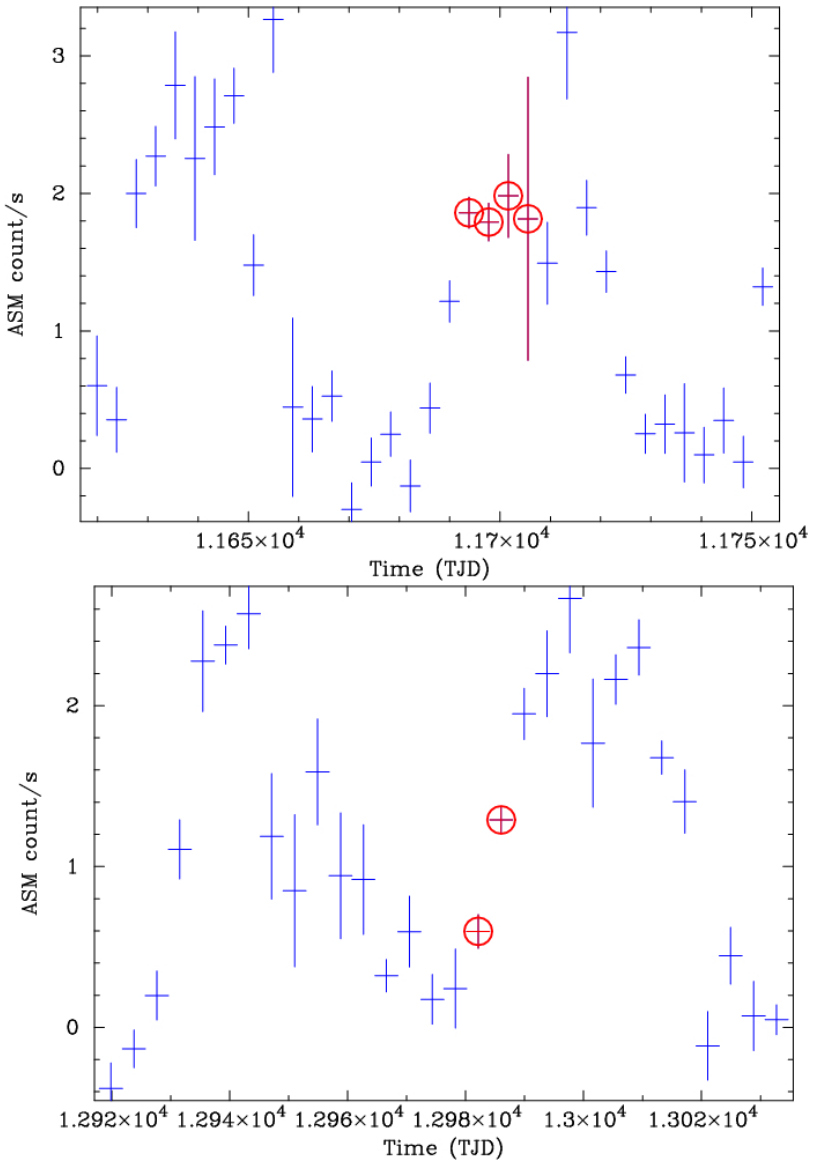

Figure 2.8 Upper panel shows the ASM light curve of SMC X-1 during the 2000 observations and the lower panel shows the ASM light curve of SMC X-1 during the 2003 observations. The points marked with red circles show the time when the PCA observations were carried out during 2000 and 2003 respectively

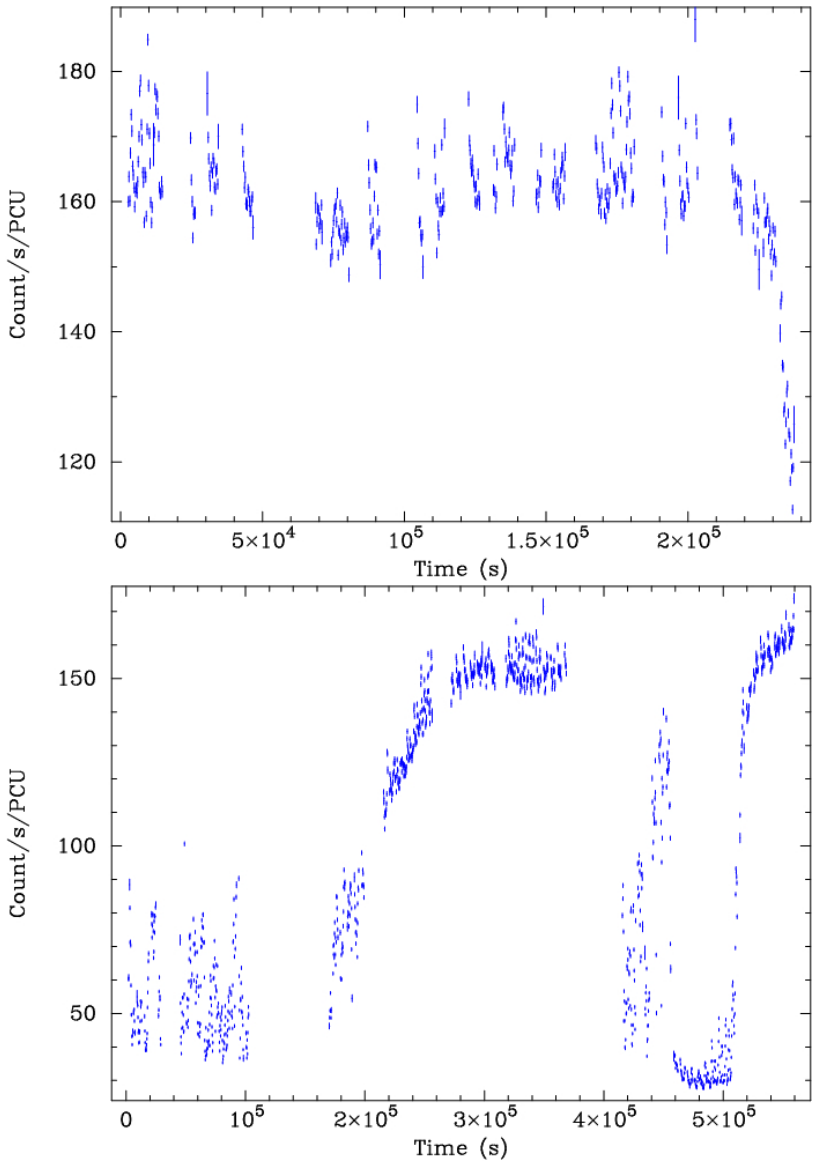

Figure 2.9 Figure shows light curves of SMC X-1. Light curve shown in the upper panel is made from the Standard-2 mode data of the 2000 observation and light curve shown in the bottom panel is made from the Standard-2 mode data of the 2003 observation

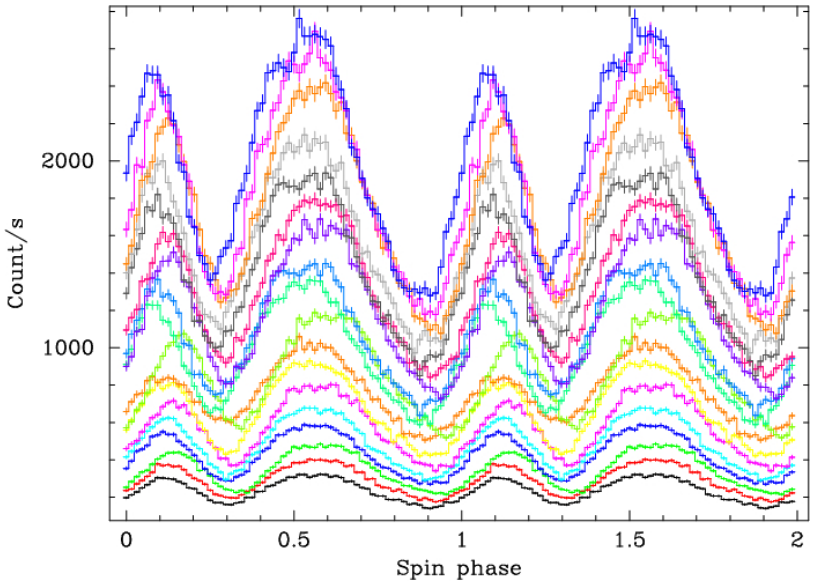

Figure 2.10 Pulse profiles of SMC X-1 for all the 12 pointed observation of RXTE for the year 2000 are shown. The original profiles have been multiplied by a constant to separate out the profiles in the presentation. There are no drastic variations in the pulse profiles. Thousand consecutive pulses were folded together with the local spin period to generate each pulse profile.

We also looked at the energy dependent pulse profiles. Figure 2.10 shows the pulse profile at different energy ranges. The overall pulse shape does not show any marked variations except that at higher energies the amplitude of both the main and the secondary peak are similar unlike that at the lower energies where the amplitude of secondary peak is smaller than the main peak. The pulsed fraction decreases at higher energy ranges and no pulsations are seen above 26 keV. We have used the full energy range from 1 keV to 60 keV covered by RXTE-PCA for measuring the arrival time delays of the pulses. The analysis procedure used is similar for both the 2000 and the 2003 observations.

2.3.2 Timing analysis

Timing analysis as described here is similar for both 2000 and 2003 observations. Light curves of time resolution of 16 ms are first generated using the event mode data. Observation done during the X-ray eclipses were not used for further analysis. The photon arrival times in the light curves were corrected to the solar system barycenter. Pulse profiles at different

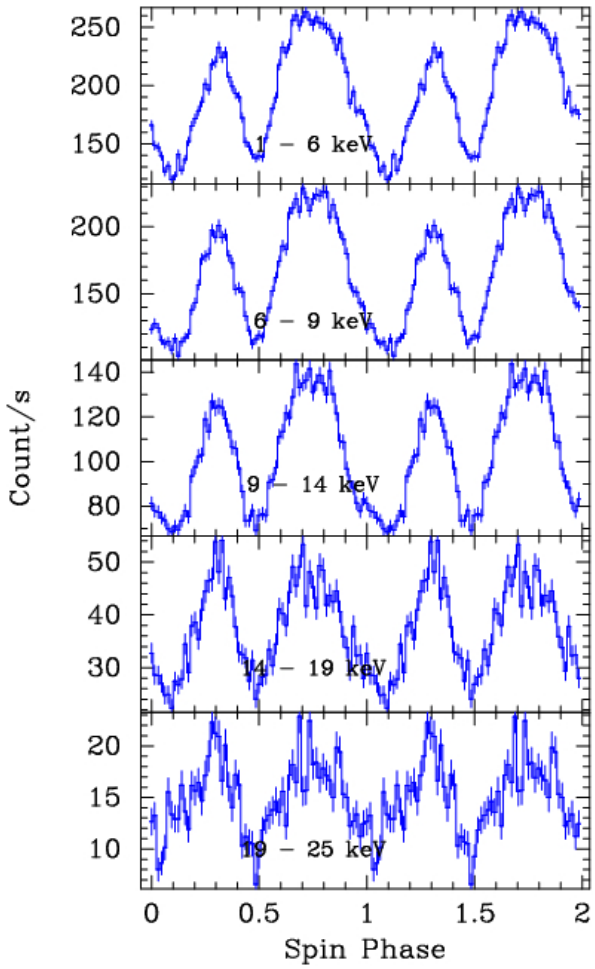

Figure 2.11 Pulse profiles of SMC X-1 in different energy bands are shown. At lower energies the second peak of the pulse profile is shorter in amplitude compared to the first peak. At higher energies both the peaks in the pulse profile have similar amplitude.

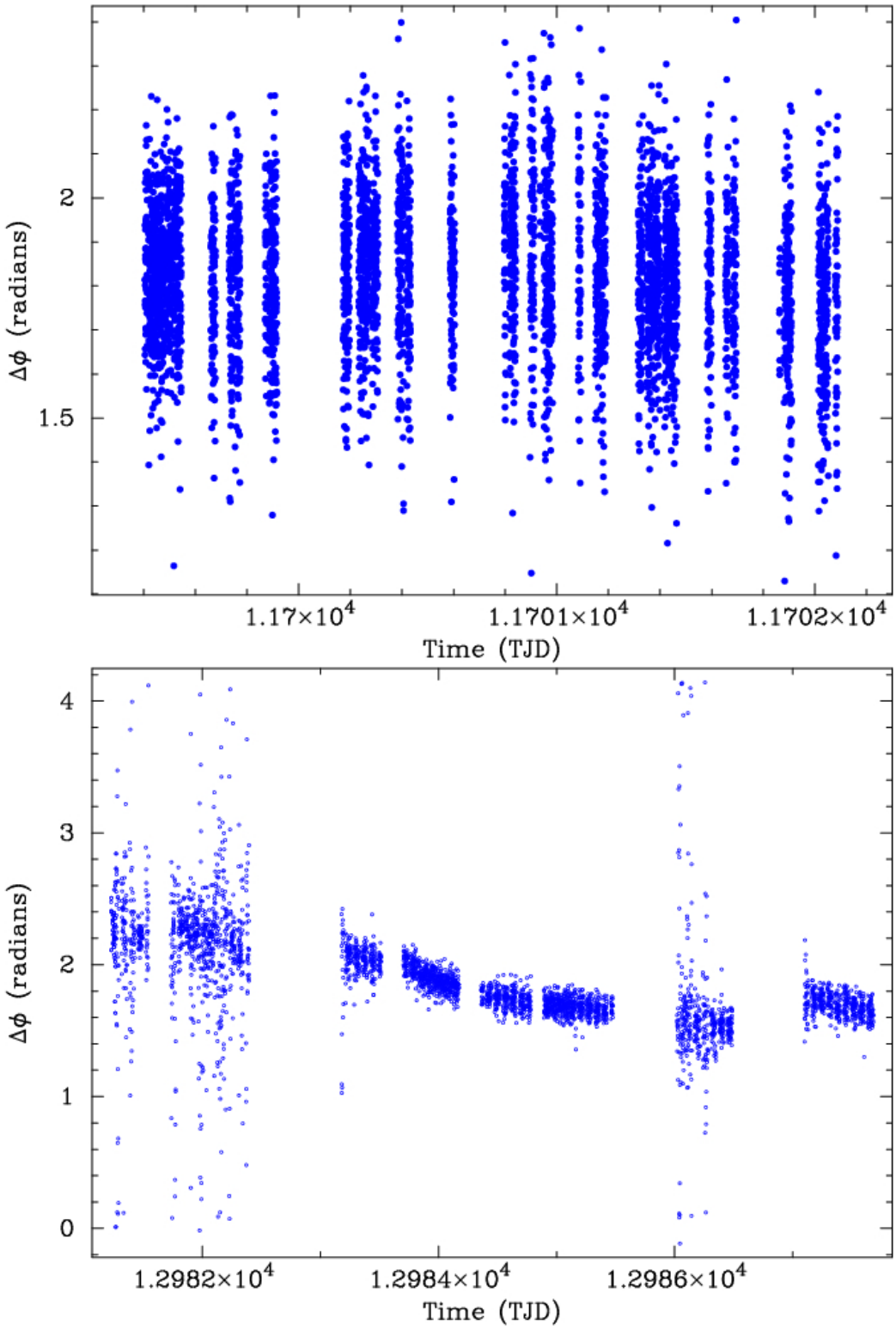

Figure 2.12 Difference in spin phase of primary peak and secondary peak $\Delta\phi$ of SMC X-1 is plotted as a function of observation time. No systematic structure is seen in the 2000 observations. The 2003 observations show larger values of $\Delta\phi$ and there are also some systematic variations. All data points that lie in the orbital phase of X-ray eclipse have been removed.

orbital phases were generated by folding twenty consecutive pulses. Each pulse profile was Fourier transformed. The phase of the Fourier component with the highest power was used to get the arrival time of that pulse profile. Arrival time is computed by the product of the phase and the spin period with which the light curve was folded to get the pulse profile. Figure 2.13 shows the arrival time delay curve for the 2000 observations and Figure 2.15 shows the same for the 2003 observations.

The delay curve generated using the 2000 observation (Figure 2.13) was used to solve equation 2.3. The values measured of the free parameters, $a_x \sin i$ and E_{2000} are given in Table 2.5. The residual delays in the arrival time of pulses were computed by subtracting the calculated circular orbit delays from the observed delays. Figure 2.14 shows the residual delays in pulse arrival times. The sinusoidal variations with a period of half the orbital period are due to the small eccentricity of the SMC X-1 orbit. This residue was used to solve the equation 2.4. The third and sixth terms in equation 2.4 are not used. The third term is due to a uniform rate of change of spin period. As there is no spin period evolution during this observation this term was dropped. The sixth term gives correction to the orbital period. But orbital period measurements done using the orbit ephemeris history are more accurate than we can derive using data covering only one binary orbit. So we have frozen the orbital period to the value reported in literature. Thus there are only six free parameters, the last two of which will give the eccentricity and ω values. Fitting the residual curve with a constant gives a reduced χ^2 of 1.34 whereas fitting it with equation 2.4 gives a reduced χ^2 of 1.082. The measured values of eccentricity and ω are given in Table 2.5.

The delay curve generated using the 2003 observation is shown in Figure 2.15. Due to the pulse profile variations as evident from the Figure 2.12b we cannot use the full delay curve to solve for equation 2.3. We therefore use only the delays measured from TJD 12983 to TJD 12985.5. The values of $a_x \sin i$ and E_{2003} measured from this segment are kept frozen. When the circular orbit delays calculated using these values of $a_x \sin i$ and E_{2003} are subtracted from the measured arrival delays we get the residues shown in Figure 2.16. The residual delays show a quadratic residue before TJD 12982.5 and after TJD 12987 which can be due to a constant

Table 2.4 SMC X-1 orbital epoch history

Orbital Cycle	Time MJD	Reference
-481	40963.99 ± 0.02	Scherier et al. 1972
-144	42275.65 ± 0.04	Tuohy & Rapley 1975
0	42836.1828 ± 0.0002	Primini et al. 1977
42	42999.6567 ± 0.0016	Davison 1977
72	43116.448 ± 0.0022	Bonnet-Bidaud et al. 1981
1055	46942.47237 ± 0.0015	Levine et al. 1993
1173	$47401.744476 \pm 0.000007$	Levine et al. 1993
1260	47740.35906 ± 0.00003	Levine et al. 1993
1464	48534.34786 ± 0.00035	Wojdowski et al. 1993
1556	48892.4191 ± 0	Wojdowski et al. 1993
1610	49102.59109 ± 0.00082	Wojdowski et al. 1993
1619	49137.61911 ± 0.00050	Wojdowski et al. 1993
1864	50091.170 ± 0.063	Wojdowski et al. 1993
2276	51694.673022 ± 0.00001	Present work
2606	52979.0174 ± 0.001	Present work

rate of change of spin period. Since the residual delays have large scatter and also show other variations which can arise due a changing pulse profile we cannot measure any eccentricity or ω from this data set.

We use the orbital ephemeris measured from the 2000 and 2003 observation to measure the orbital period and rate of orbit decay. Table 2.4 tabulates the history of SMC X-1 orbital ephemeris. The orbital period and $\dot{P}_{orb}/P_{orb}$ measured by combining all the measured E_n's are given in Table 2.5. The orbit decay of SMC X-1 is also explained as arising due to the tidal interaction of SMC X-1 neutron star and the companion star (SK 160). Levine et al. (1993) have shown by Monte Carlo evaluations that the asynchronism in this system is maintained because of the evolution of SK 160 which at the present time is in its shell hydrogen-burning phase. Due to shell hydrogen-burning the star is rapidly expanding which increases the moment of inertia of the companion. This increase in moment of inertia will decrease the rotational angular momentum giving rise to the asynchronism needed for tidal dissipation of orbital angular momentum.

Table 2.5 SMC X-1 orbit parameters

Parameter	Value	
	2000	2003
$a_x \sin i$	53.5769 ± 0.0006 (lt-sec)	53.339 ± 0.032 (lt-sec)
E	$51694.673697 \pm 0.000012$ (MJD)	52979.0159 ± 0.0022 (MJD)
e	0.00021 ± 0.00001	–
ω	$-43^0.23 \pm 8^0.99$	–
E_0	42836.1827 ± 0.0003 (MJD)	
P_{orb}	3.89229263 ± 0.0000004 d	
$\dot{P}_{orb}/P_{orb}$	$-(3.414 \pm 0.003) \times 10^{-6} yr^{-1}$	

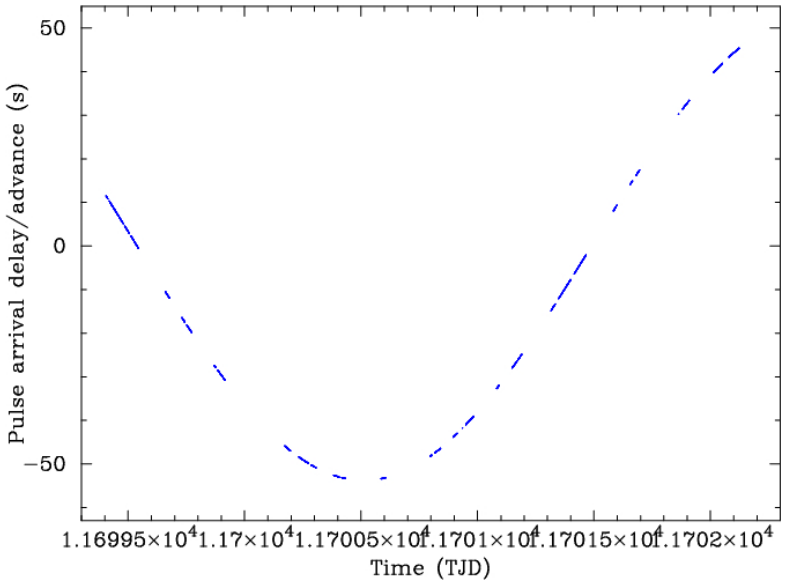

Figure 2.13 Figure shows the pulse arrival time delay curve of SMC X-1 obtained using the 2000 RXTE-PCA observations

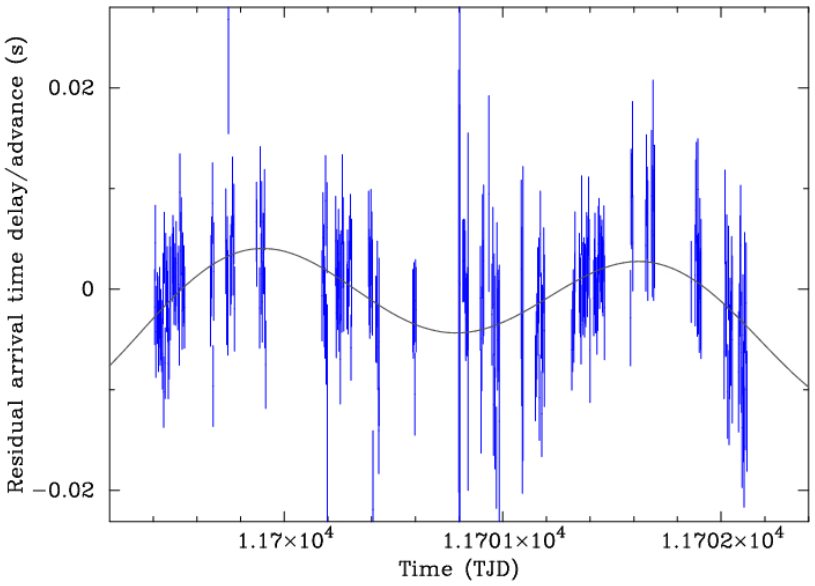

Figure 2.14 Figure shows the residual pulse arrival delays/advance of SMC X-1 pulses after subtracting delays expected by a circular orbit from the observed delays obtained using the 2000 RXTE-PCA observations. For clarity 20 consecutive data points have been averaged to get one data point of this curve.

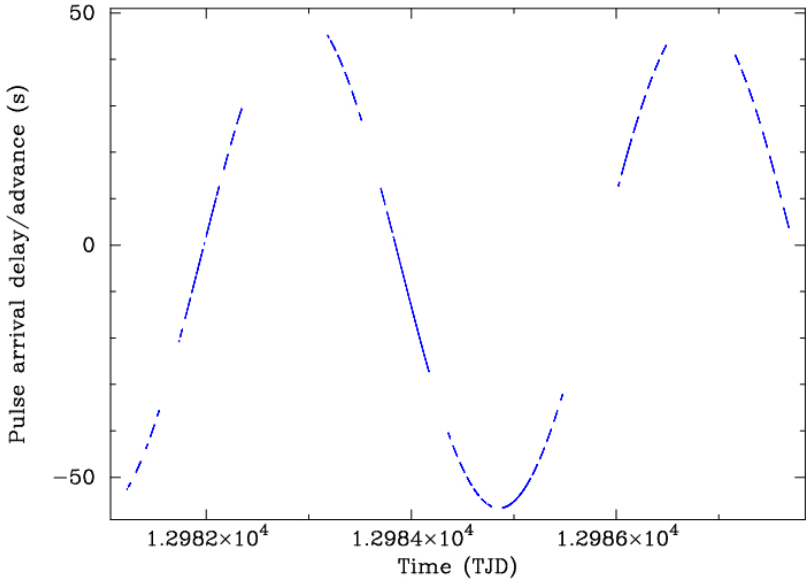

Figure 2.15 Figure shows the delay curve of SMC X-1 obtained using the 2003 RXTE-PCA observations

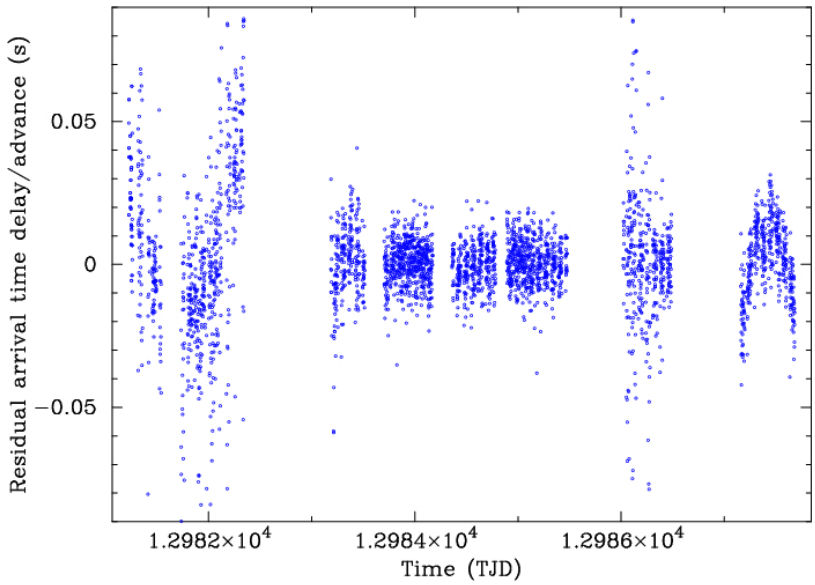

Figure 2.16 Figure shows the residual pulse arrival delays/advance of SMC X-1 pulses after subtracting delays expected by a circular orbit from the observed delays. The error bars are not shown for clarity reasons.

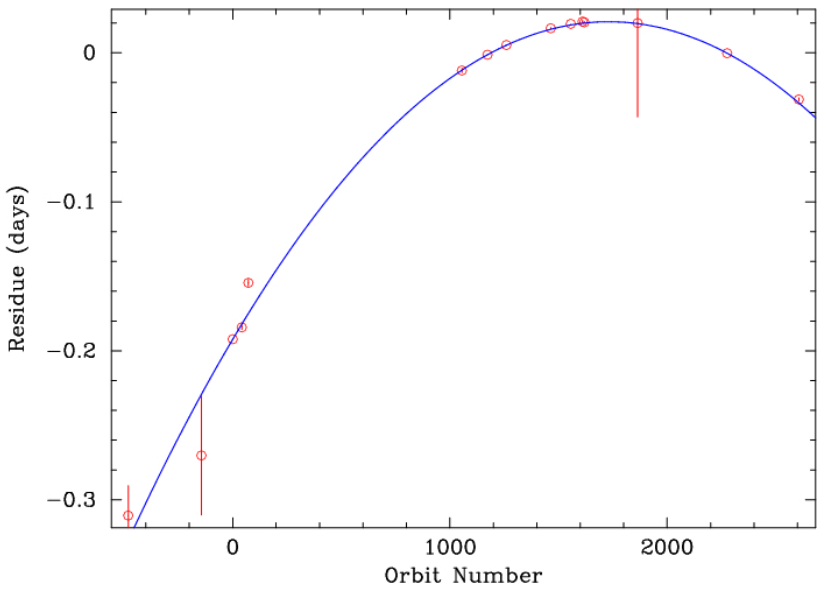

Figure 2.17 The observed-minus-calculated eclipse times for SMC X-1 are plotted with respect to the orbit number. The quadratic trend due to orbital period decay is clearly seen. The solid curve represents the best-fit to a constant rate of orbital decay.

2.4 4U 1538–52

4U 1538–52 is an X-ray pulsar, first detected with the UHURU satellite (Giacconi et al. 1974). Regular X-ray pulsations with a period of 529 s were later discovered with Ariel 5 and OSO-8 observations by Davison et al. (1977). In addition, the OSO-8 observations revealed a clear orbital modulation of the pulsation period and also showed good evidence for an eclipse lasting 0.6 day recurring with a period of 3.75 days. The optical counterpart was found to be an early B type supergiant star with H-alpha emission lines (Parkes et al. 1978). Features in the optical spectrum suggested a distance to the source of $\sim$ 5.5 kpc and the mass-loss rate for the companion was estimated to be $\sim 10^{-6}$ $M_{\odot}$ yr^{-1}.

Makishima et al. (1987) using TENMA and Robba et al. (1992) using EXOSAT observed pulse periods of $\sim$ 530 s with an average spin-down rate of $\dot{P} \sim 3.9 \times 10^{-9}$ s s^{-1}. Subsequently, the Burst and Transient Source Experiment (BATSE) onboard the Compton Gamma Ray Observatory (CGRO) detected a reversal of the long term spin down to spin up, probably in 1988 (Rubin et al. 1997), which has also been confirmed by BeppoSAX (Robba et al. 2001). The spectrum has an iron K fluorescence line at 6.4 keV, a cyclotron absorption line near 20 keV and is well fitted with a power law and high energy cut-off at $\sim$ 16 keV (Clark et al. 1990, Robba et al. 2001). X-ray eclipse phenomena were investigated by Clark, Woo and Nagase (1994) with the GINGA data.

2.4.1 Observations and Timing Analysis

We observed the source with the Proportional Counter Array (PCA) of RXTE from 2003-07-31 to 2003-08-07 covering the out of eclipse phases for two binary orbits. There were twenty-five observations, each corresponding to one orbit of the satellite. Each observation was of 1.5–6.0 ks duration. On an average, three PCUs were ON for the observations in 2003. We extracted light curves from the event mode data with time resolution of 0.125 s. Only photons detected in the top two layers were used. The photon arrival times were then corrected to the solar system barycenter. Figure 2.18 shows the complete barycentered light curve for the August 2003 observation with RXTE-PCA.

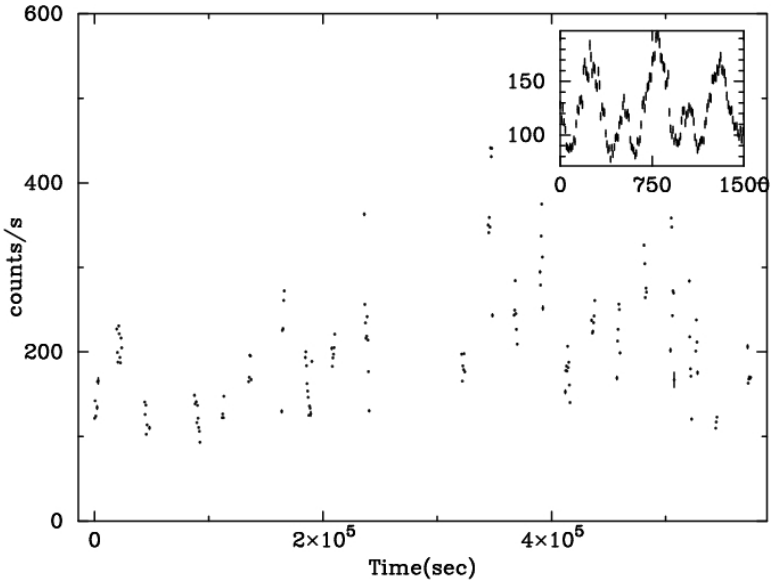

Figure 2.18 Figure shows complete barycenter corrected light curve of 4U1538–52 for the August 2003 observations with a time resolution of 100 s. The inset is an expanded view of part of the light curve with a time resolution of 10 s. Pulsations of period 526.84 s are seen clearly.

The light curve shows variability at time scales other than the regular 526.85 s pulses from the neutron star. The pulsed emission is strong enough for individual pulses to be seen in the energy range from 1 keV to 40 keV. The pulse profile is double peaked with a main pulse and an inter pulse which is about half the amplitude of the main pulse. The average pulse period of the source was obtained by pulse folding and χ^2 maximisation method.

The light curve was then folded with the average spin period derived to get pulse profiles at different orbital phases. Each pulse profile is an average of two successive pulses binned into 256 pulse phase bins. A total of forty six such pulse profiles were generated, spanned over two binary orbits of 4U 1538–52. To get the arrival times of these pulses, we decomposed each pulse profile into 128 Fourier components. The phase of the first Fourier component which also has the highest amplitude was used to find the arrival time delay of the respective pulses. Figure 2.19a shows the arrival time delay curve.

The arrival time delay curve when fitted with a circular orbital delay curve (i.e. $e = 0$) leaves out systematic residues as shown in Figure 2.19b indicating an elliptical orbit. Subsequently,

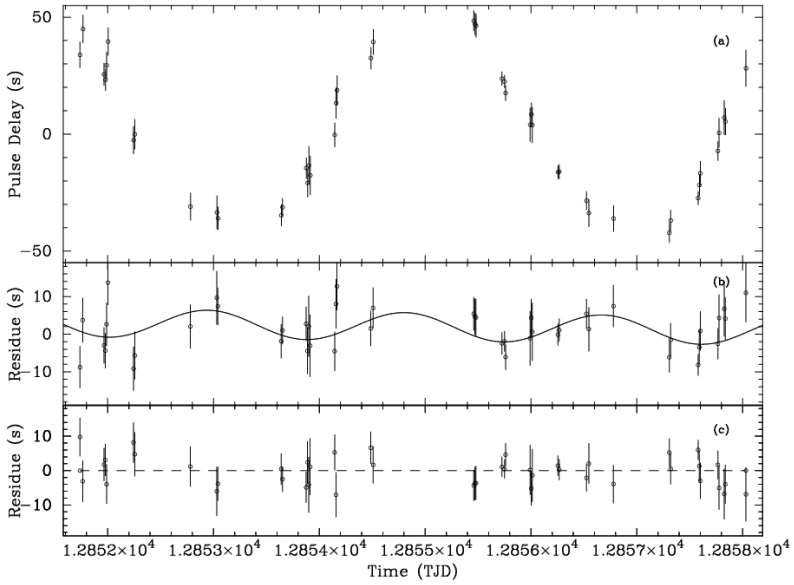

Figure 2.19 Figure shows (a) measured delays in pulse arrival time for the binary system 4U 1538-52 obtained using the 2003 RXTE-PCA observations (b) Residual delays after subtracting expected delays due to a circular orbit (c) Residual delays in arrival times after subtracting expected delays due to an eccentric orbit

we fitted the pulse arrival time delay with a function appropriate for elliptical orbit given below.

$$\Delta t = \frac{a_x \sin i}{c}(1-e^2)\frac{\sin(\nu+\omega)}{1+e\cos\nu} \tag{2.6}$$

$$\tan\frac{\nu}{2} = \sqrt{\frac{1+e}{1-e}}\tan\frac{E}{2} \tag{2.7}$$

$$E - e\sin E = \frac{2\pi}{P_{orb}}(t - T_0 - \frac{P_{orb}}{2\pi}\omega) \tag{2.8}$$

$$T_0 = T_{\pi/2} - \frac{P_{orb}}{4} \tag{2.9}$$

It was seen that the errors in the individual measurements of pulse arrival times were greater than the error due to photon counting statistics, possibly due to some aperiodic intensity variation over a range of time scales. While fitting the arrival delay curve to an elliptical binary orbit, the statistical uncertainties on the arrival time measurements were multiplied by a constant factor to obtain a reduced χ^2 value of 1.0. This method was employed so that one

can compare the orbital parameter estimations with the earlier measurements (Clark 2000). For a circular orbit, the rescaled uncertainties gives a best fit with a χ^2 value of 64 for 43 degrees of freedom. Comparing this with the reduced χ^2 value of 1 for an elliptical orbit as described above, we reconfirm an elliptical orbit for this system. The value of the five free parameters for an elliptical fit, namely P_{spin}, $a_x \sin i$, e, ω, and $T_{\pi/2}$ are listed in Table 2.6. We combined the new epoch measured from the RXTE data taken in 2003 with the earlier measurements listed in Table 2.7. The mid-eclipse times derived from light curves obtained using the UHURU and ARIEL V were not included because the X-ray eclipse is asymmetric as seen in the folded ASM light curve of Figure 2.20. As the X-ray source goes into eclipse gradually and comes out of the eclipse rather sharply, the mid-eclipse time determined from the light curve only is likely to be inaccurate and have some systematic errors. Fitting the remaining 9 mid-eclipse times with a linear function gives a reduced χ^2 of 1.3 for 7 degrees of freedom. The residuals from a linear fit to the mid-eclipse times are shown in Figure 2.21. A quadratic fit improves the reduced χ^2 by a mere 0.01 (for 6 degrees of freedom). If the mid-eclipse time record is fitted with an orbital evolution corresponding to the value reported in Clark (2000), a reduced χ^2 of 2.5 is obtained, which is larger than the same for a linear fit. We, therefore, conclude that there is no evidence for an orbital evolution in 4U 1538–52 from the available data.

2.4.2 Conclusions

A pulse period of 526.85 s of the pulsar 4U 1538–52 determined from RXTE-PCA observation in 2003 shows that the spin-up trend of 4U 1538–52 first detected with BATSE during the 1990s has continued since then. The overall spin-up time scale ($\dot{P}/P$) during the five years of BATSE observation reported by Rubin et al. (1997) was 9.6×10^{-12} s^{-1}. The average spin-up rate between the end of BATSE observations and the later observations with RXTE (1997, Clark 2000), Beppo-SAX (1998, Robba et al. 2001) and again with RXTE (2003, present work) is 1.4, 1.2 and 7.4×10^{-11} s^{-1}, significantly larger than the average spin-up rate during the BATSE era. An increase in spin-up rate is expected if the overall X-ray luminosity had

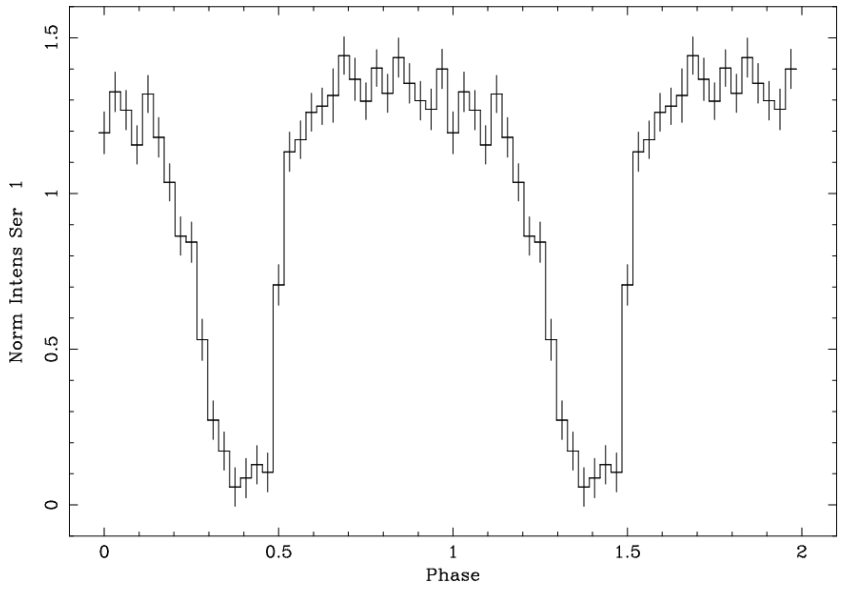

Figure 2.20 RXTE-ASM light curve of 4U 1538-52 folded at the orbital period of 3.73 days. Two cycles are shown.

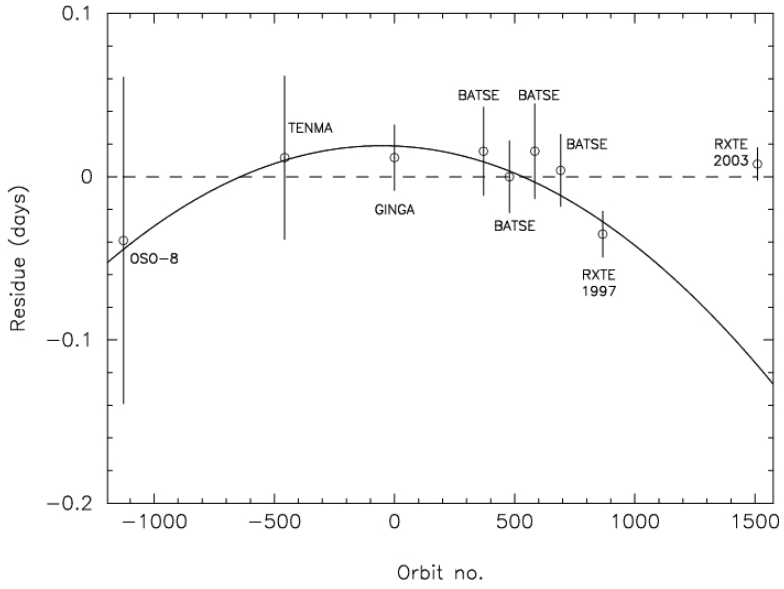

Figure 2.21 Residual mid-eclipse times are shown after subtracting the linear trend. Solid line indicates the quadratic fit of mid-eclipse times till the 1997 observations (Clark et al. 2000)

Table 2.6 These are the parameters measured by an elliptic fit. The errors quoted are 1σ errors.

Parameter	Value
P_{spin}	526.849 ± 0.003 s
$a_x \sin i$	53.05 ± 1.45 lt-s
e	0.18 ± 0.01
ω	$39^o.47 \pm 12$
$T_{\pi/2}$	52851.33 ± 0.01 MJD
a_o	47221.463 ± 0.012
P_{orb}	3.728382 ± 0.000011

$T_{\pi/2}(N) = a_0 + P_{orb}N$

increased after the BATSE observations. However, it is very impractical to compare the pulsed hard X-ray flux measured by BATSE and the total X-ray flux measurements with the later instruments in a different energy band.

The value of $a_x \sin i$ that we obtained from pulse timing of the RXTE-PCA data in 2003 is 53.1 ± 1.5 lt-s, which is consistent with the BATSE result and slightly smaller than that obtained from the 1997 RXTE data. We note here that the accuracy of orbital parameter determination in slow pulsars like 4U 1538–52 is considerably poorer than in fast pulsars like SMC X-1, Her X-1 etc. In analysis of the BATSE data, Rubin et al. (1997) considered a circular orbit whereas analysing pulse arrival times from two complete binary orbits we found the orbit of 4U 1538–52 to be eccentric with e = 0.18 ± 0.01. Our result is consistent with the results obtained from a 1997 observation of this source with the RXTE-PCA (Clark 2000). The value of ω determined from the 2003 observation is smaller compared to that found by Clark from the 1997 observation. If the difference is due to apsidal motion then the rate of apsidal motion is $\dot{\omega} = -3.8^o \pm 2^o.2$ yr^{-1}. We found no significant evidence for orbital evolution in the system as reported from earlier measurements (Clark 2000). The value of $\dot{P}_{orb}/P_{orb}$ determined from all the available mid-eclipse times is $(2.5 \pm 1.9) \times 10^{-6}$ yr^{-1}. Combining the pulse timing results on 4U 1538–52 obtained from our observation with the earlier reported

Table 2.7 Measured mid-eclipse times for 4U 1538–52

Orbit Number	Epoch (MJD)	Reference
-1128	43015.800 ± 0.100	Becker et al. 1977
-457	45517.660 ± 0.050	Makishima et al. 1987
0	$47221.474 \pm .020$	Corbet et al. 1993
370	48600.979 ± 0.027	Rubin et al. 1997
478	49003.629 ± 0.022	Rubin et al. 1997
584	49398.855 ± 0.029	Rubin et al. 1997
691	49797.781 ± 0.022	Rubin et al. 1997
866	50450.206 ± 0.014	Clark 2000

$T_{\pi/2}(N) = a_0 + P_{orb}N$

measurements, we are able to rule out an orbital decay in this system for which Clark (2000) found marginal evidence. The new upper limit presented here on possible changes of the orbital period of 4U 1538–52 supersedes previous limits considerably.

Tidal interaction between the two stars and mass loss from the companion star are the two main effects that cause orbital decay in the HMXB systems. The companion star mass, and the size of the binary orbit in 4U 1538–52 is very similar to the above mentioned binaries, and therefore, the tidal effect that is expected in 4U 1538–52 should be as strong as in the three other HMXBs. But we find no clear evidence of an orbital decay in 4U 1538–52. If at all, the system shows a positive orbital period derivative, like the enigmatic system Cyg X-3 (Singh et al. 2002). This indicates that mass loss may play a prominent role in the evolution of this system. Tidal interaction between the neutron star and the companion in close HMXBs should also circularise the orbit. The orbits of most of the close (orbital period less than 4 days) HMXBs are highly circularised with eccentricity less than 0.006. But the orbit of 4U 1538–52 is not yet circularised and shows no orbital decay. Therefore, it is likely that 4U 1538–52 is a relatively young system compared to the other HMXBs. Using the mass, radius and luminosity of the companion star QV Nor from the optical observation (Reynolds et al. 1992) the approximate time for tidal circularisation of this system works out to be 2×10^3

yrs (Lecar, Wheeler & McKee,1976). Since the system is still eccentric, it is possible that the age of the system after the supernova explosion is of the order of a few thousand years; very small compared to the lifetime of HMXBs.

The eccentricity derived using the two RXTE observations in 1997 (Clark 2000) and 2003 (reported here) is likely to be correct for two reasons. The RXTE-PCA has a large effective area compared to the earlier missions and in the energy range of PCA more photons are detected compared to CGRO-BATSE using which Rubin et al (1997) did not detect any eccentricity. If the eccentricity is high, then either the binary system is young or the circularisation time is actually much longer than a few thousand years estimated using Lecar's method (1976). On the other hand, a binary is unlikely to become very X-ray active by wind accretion within just a few thousand years of the supernova explosion. It is possible that the circularisation mechanism works very efficiently in systems with Roche-lobe overflow like LMC X-4 while accretion mechanism in 4U 1538–52 is likely to be driven by stellar wind.